A modified fundamental measure theory for spherical particles in microchannels

Yang-Xin Yu
Department of Chemical Engineering, Tsinghua University, Beijing 100084, People's Republic of China

Jianzhong Wu[a)]
Department of Chemical and Environmental Engineering, University of California, Riverside, California 92521-0425

Canonical-ensemble Monte Carlo simulation and an improved fundamental-measure theory are applied to calculating the structures and chemical potentials of neutral and associating spherical particles confined in rectangular or corrugated microchannels. It is found that the confinement significantly affects the distributions of neutral spheres in the microchannels, especially at high densities or near the confining surfaces. However, for associating particles, the combined effects of packing and association lead to virtually uniform density distributions. The density profiles calculated from the density functional theory agree well with simulation results for neutral hard spheres in both rectangular and corrugated microchannels except when the average packing density inside the channel is near the freezing point. © *2003 American Institute of Physics.*
[DOI: 10.1063/1.1584426]

I. INTRODUCTION

The structure of colloids in confining geometry is closely related to the self-assembly of colloidal particles for material applications and to the flow behavior of colloids through micropores or channels. For instance, close packed monodisperse silica or latex nanoparticles have been proposed for applications in microphotonic crystal devices and chips.[1] Understanding the fundamental mechanisms that drive the assembly of particles at microscopic level will bring about new strategies for the fabrication of well-ordered arrays of nanoscale objects. On the other hand, transport of colloids through pores of colloidal dimensions is commonplace in nature especially in biological systems such as blood streams and milk.[2] Investigations on the static density distribution of confined colloids provide a useful starting point for understanding the microscopic flow behavior. Recently, colloidal dispersions in confining geometry have also attracted considerable theoretical interest as model systems for studying the adsorption and phase transitions in reduced dimensionalities.[3,4] It has been found that the phase behavior of a confined fluid can be drastically different from that of a bulk fluid.[5]

Both Monte Carlo (MC) simulation and density functional theory (DFT) are commonly used to study the density distributions and thermodynamic properties of confined systems. Typically, simulation methods are based on the grand canonical ensemble (GCE) because a confined system is conventionally specified by temperature, volume and the chemical potentials of all species. Whereas there have been extensive investigations on the properties of fluids with only one-dimensional inhomogeneity such as fluids in slit pores,

cylindrical pores or spherical cavities,[6–10] relatively few studies have been reported on fluids confined in more complicated geometries.[11,12] For systems with two-dimensional inhomogeneity in particular, Schoen and Dietrich used GCE–MC to analyze the entropy-driven structure formation of hard spheres in the groove of furrowed hard substrates.[13] They observed that at sufficiently high packing densities, the furrow leads to a solidlike order of fourfold in-plane symmetry. Henderson and co-workers found that the density distributions from GCE–MC simulations are in good agreement with the predictions of the Tarazona's DFT.[11] Very recently, Jagannathan and Yethiraj[12] applied GCE–MC simulation and the DFT of Curtin and Ashcroft[14] to calculating the density distributions of hard spheres in square and rectangular channels.[12] It was observed that the two-dimensional confinement could introduce both constructive and destructive interferences in the density profiles near the corners of microchannels. Other simulation methods, including canonical ensemble (NVT), Gibbs ensemble (GE), and isobaric–isothermal ensemble (NPT), have also been reported for investigating the structure and phase behavior of confined fluids.[15] However, straightforward application of GCE or GE methods is limited to systems with relatively low densities. At a density near the freezing transition, a lengthy simulation, up to 1000 million simulation steps per particle, is often required to attain accurate density distributions and thermodynamic properties.[16] Whereas NVT and NPT methods avoid particle insertions, these methods do not provide the chemical potential of confined systems, a quantity of central importance in phase-equilibrium calculations. Calculation of chemical potential using the conventional Widom's method[17] also relies on the insertion of test particles, which is again limited to systems of relatively low densities.

Among various density functional theories of classical

[a)]Author to whom correspondence should be addressed. Electronic mail: jwu@engr.ucr.edu

systems, the fundamental measure theory (FMT) by Rosenfeld probably gives the most accurate structural and thermodynamic properties of inhomogeneous hard-sphere fluids.[18,19] This theory assumes that the excess intrinsic Helmholtz energy can be expressed in terms of weighted densities that take into account the geometric feature of a spherical particle. Because the weight functions are independent of density distributions, FMT is numerically more convenient to implement than most other nonlocal density-functional theories. Recently, we have reformulated the fundamental-measure theory based on the Boublik–Mansoori–Carnahan–Starling–Leland (BMCSL) equation of state.[20–22] This modification leads to improvements on both density distributions and the adsorption isotherms of spherical particles, especially at high packing densities.[23]

In this work, we apply the NVT ensemble Monte Carlo simulation and the improved fundamental-measure theory to investigating the structures and adsorption isotherms of neutral hard spheres and associating hard spheres in microchannels of different geometries. For comparison with the prediction of the DFT, the chemical potentials in Monte Carlo simulation are calculated using a modified Widom's insertion method.[23] Because the excess chemical potential is extrapolated from those for smaller testing hard spheres, this simulation method is applicable to systems with high packing densities.

II. NVT SIMULATION OF CONFINED HARD SPHERES

We consider N hard spheres of uniform diameter σ confined in a rectangular channel of length $L=(l+1)\sigma$ in the x direction and $H=(h+1)\sigma$ in the y direction. Periodic boundary conditions are imposed in the z direction. The geometry of the rectangular channel is fixed at $l=14$ and $h=9$ and the average density of hard spheres within the channel varies from $\rho\sigma^3=0.42$ to 0.93, all below the freezing density of hard spheres in the bulk. We assume that the microchannel consists of structureless hard walls with no attraction to the confined particles.

The conventional Metropolis algorithm is used for generating successive configurations with the probability of successful displacement adjusted to 50%. At each density, the simulation box contains 1001 particles and the simulation is run for 2.1×10^8 Monte Carlo step (MCS) for sampling the density distributions after about 1×10^6 MCS per particle for equilibrium. The density profiles are recorded with a fixed bin size of 0.025σ.

Along with the density profiles, the excess chemical potential of hard spheres is calculated using a modified Widom's insertion method proposed by Labik and Smith.[23] In this method, the excess chemical potential of a large particle is extrapolated from those for a range of smaller particles. According to the scale-particle theory,[24] the excess chemical potential of a hard-sphere fluid can be related to the work to insert a particle into the system, which is proportional to the particle volume and surface area. It follows that the excess chemical potential of a hard testing particle can be represented as a third-order polynomial of the particle diameter d approximately

$$\mu^e_{av}(d)/k_BT=\sum_{i=0}^{3} a_i d^i, \qquad (1)$$

where k_B stands for the Boltzmann constant and T for temperature. The coefficients a_0, a_1, a_2 and a_3 are independent of hard-sphere diameter and can be obtained by fitting Eq. (1) to the excess chemical potential of smaller particles calculated using Widom's insertion method.[17] By extrapolating the diameter of the inserted particle to the hard sphere diameter σ, Eq. (1) allows us to obtain the excess chemical potential of confined hard spheres at relatively high densities.

III. DENSITY FUNCTIONAL THEORY FOR HARD SPHERES AND ASSOCIATING HARD SPHERES

The essential task of a density functional theory is to provide an analytical expression for the intrinsic Helmholtz energy $F[\rho(\mathbf{r})]$ as a functional of the density distribution $\rho(\mathbf{r})$. For a one-component system with a given chemical potential μ in an external potential $V_{ext}(\mathbf{r})$, the equilibrium density distribution satisfies the Euler–Lagrange equation

$$\mu-V_{ext}(\mathbf{r})=\delta F[\rho(\mathbf{r})]/\delta\rho(\mathbf{r}). \qquad (2)$$

With an expression for the intrinsic Helmholtz energy $F[\rho(\mathbf{r})]$, the density distribution $\rho(\mathbf{r})$ can be solved from Eq. (2), and subsequently both structural and thermodynamic properties can be calculated in principle.

In this work, we consider neutral and associating hard spheres confined in microchannels. The intrinsic Helmholtz energy includes an ideal part $F_{id}[\rho(\mathbf{r})]$ that is known exactly

$$F_{id}[\rho(\mathbf{r})]=k_BT\int d\mathbf{r}\,\rho(\mathbf{r})\{\ln(\rho(\mathbf{r})\lambda^3)-1\}, \qquad (3)$$

and an excess part $F_{ex}[\rho(\mathbf{r})]$ that takes into account the excluded-volume effect and interparticle associations. In Eq. (3), λ stands for the thermal wavelength of a particle. Conventionally, it is postulated that the excess intrinsic Helmholtz energy functional can be expressed as

$$F_{ex}[\rho(\mathbf{r})]=k_BT\int d\mathbf{r}\,\Phi[\rho(\mathbf{r})], \qquad (4)$$

where the excess intrinsic Helmholtz energy density $\Phi[\rho(\mathbf{r})]$ is a function of $\rho(\mathbf{r})$. For the systems considered in this work, $\Phi[\rho(\mathbf{r})]$ consists of contributions from hard-sphere repulsion (hs) and interparticle associations (assoc),

$$\Phi[\rho(\mathbf{r})]=\Phi^{hs}[\rho(\mathbf{r})]+\Phi^{assoc}[\rho(\mathbf{r})]. \qquad (5)$$

In the limit of a uniform fluid, $V_{ext}(\mathbf{r})=0$ and $\rho(\mathbf{r})=\rho$, the excess intrinsic Helmholtz energy reduces to the conventional residue Helmholtz energy, and $\Phi[\rho(\mathbf{r})]$ becomes the residue Helmholtz energy per unit volume.

We use a modified fundamental-measure theory to represent the excess intrinsic Helmholtz energy density due to hard-sphere collisions.[22] In our previous work, we have shown that this DFT theory provides an accurate description of density distributions of hard spheres near hard walls and in hard slit pores. In addition, it predicts accurate direct and pair correlation functions of uniform hard spheres including those for highly asymmetric hard-sphere mixtures. As in the original fundamental-measure theory proposed by

Rosenfeld,[18,19] the hard-sphere intrinsic Helmholtz energy density includes contributions from scalar weighted densities (denoted by the superscript S) and vector weighted densities (denoted by the superscript V),

$$\Phi^{hs}[\rho(\mathbf{r})] = \Phi^S + \Phi^V, \tag{6}$$

where the scalar intrinsic Helmholtz energy density has the form of BMCSL equation for hard spheres in the bulk[22]

$$\Phi^S = -n_0 \ln(1-n_3) + \frac{n_1 n_2}{1-n_3}$$
$$+ \left[\frac{1}{36\pi n_3^2} \ln(1-n_3) + \frac{1}{36\pi n_3(1-n_3)^2} \right] n_2^3 \tag{7}$$

and the vector intrinsic Helmholtz energy density is derived from the scale-particle theory of Resonfeld[18,19]

$$\Phi^V = -\frac{\mathbf{n}_{V1} \cdot \mathbf{n}_{V2}}{1-n_3} - \left[\frac{1}{12\pi n_3^2} \ln(1-n_3) \right.$$
$$\left. + \frac{1}{12\pi n_3(1-n_3)^2} \right] n_2 \mathbf{n}_{V2} \cdot \mathbf{n}_{V2}. \tag{8}$$

As in the original fundamental measure theory, the scalar and vector weighted densities are defined as

$$n_\alpha(\mathbf{r}) = \int d\mathbf{r}' \, \rho(\mathbf{r}') \omega^{(\alpha)}(\mathbf{r}-\mathbf{r}'), \tag{9}$$

where $\omega^{(\alpha)}(\mathbf{r})$ are weight functions that characterize the geometry and surface variance of a spherical particle, and the subscripts $\alpha = 0, 1, 2, 3, V1, V2$ are the indices of the weighted densities. The weighted densities $\omega^{(3)}(\mathbf{r})$, $\omega^{(2)}(\mathbf{r})$, and $\omega^{(V2)}(\mathbf{r})$ are related to the particle volume, surface area and surface normal vector, respectively,

$$\omega^{(3)}(\mathbf{r}) = \Theta(R-r), \tag{10}$$

$$\omega^{(2)}(\mathbf{r}) = \delta(R-r), \tag{11}$$

$$\omega^{(V2)}(\mathbf{r}) = (\mathbf{r}/r)\delta(R-r), \tag{12}$$

where $\Theta(R-r)$ is the Heaviside step function, $\delta(R-r)$ is the Dirac delta function, and R is the hard-sphere radius. The other weight functions are proportional to the geometric functions given in Eqs. (10)–(12),

$$\omega^{(0)}(\mathbf{r}) = \omega^{(2)}(\mathbf{r})/(4\pi R^2), \tag{13}$$

$$\omega^{(1)}(\mathbf{r}) = \omega^{(2)}(\mathbf{r})/(4\pi R), \tag{14}$$

$$\omega^{(V1)}(\mathbf{r}) = \omega^{(V2)}(\mathbf{r})/(4\pi R). \tag{15}$$

As indicated earlier, all weight functions are independent of density distributions.

In our previous work,[25] we extended the statistical associating fluid theory (SAFT)[26] for the thermodynamic properties of bulk fluids to inhomogeneous systems. The associating fluid are modeled as a hard sphere with four associating sites placed in the Bol fashion, i.e., the four bonding sites, designated by A, B, C, and D, are placed in tetrahedral symmetry around a spherical core. Only associations between AC, BC, AD, and BD sites are allowed and all the bonding energies are assumed to be identical and the association po-

tential is modeled by an anisotropic short-range square well. In the bulk case, the Helmholtz energy density for associations is given by

$$\Phi^{assoc,b} = M\rho_b(\ln\chi_A^b - \chi_A^b/2 + 1/2), \tag{16}$$

where M is the number of association sites per molecule, χ_A^b is the fraction of molecules not bonded at site A. In Eq. (21), χ_A^b is calculated from

$$\chi_A^b = \frac{1}{1+\rho_b\Sigma_\alpha\chi_\alpha^b\Delta}, \tag{17}$$

where $\Delta = 4\pi K g^{hs,b}(\sigma)f$, K is a constant reflecting the volume available for bonding of the two sites on molecules 1 and 2, $f = \exp(\epsilon/k_B T) - 1$ represents the Mayer function, ϵ is the square-well depth for the association bonding, and $g^{hs,b}(\sigma)$ is contact value of the hard-sphere pair correlation function,

$$g^{hs,b}(\sigma) = \frac{1}{1-\xi_3} + \frac{1.5\sigma\xi_2}{(1-\xi_3)^2} + \frac{0.5\sigma^2\xi_2^2}{(1-\xi_3)^3}, \tag{18}$$

where $\xi_m = (\pi/6)\rho_b\sigma^m$, and $m = 0, 1, 2, 3$. Following our previous work,[25] we use $K = 1.4849\times10^{-4}\sigma^3$ in our calculations.

To extend Eq. (16) to inhomogeneous systems, in previous paper we replaced ξ_3, ξ_2, and ρ_b in Eqs. (16)–(18) with n_3, $\frac{1}{6}n_2\zeta$, $\frac{1}{36}n_2^2\zeta$, and $n_0\zeta$, respectively. Here $\xi = 1 - \mathbf{n}_{V2}\cdot\mathbf{n}_{V2}/n_2^2$ is used to take into account the vector-weighted densities. Subsequently, the Helmholtz energy density of association becomes

$$\Phi^{assoc}(n_\alpha) = n_0\zeta M\left[\ln\chi_A(\mathbf{r}) - \frac{\chi_A(\mathbf{r})}{2} + \frac{1}{2} \right], \tag{19}$$

where $\chi_A(\mathbf{r})$ is the fraction of the associating sites not bonded at position $\mathbf{r}$. From Eq. (17), $\chi_A(\mathbf{r})$ for a fluid containing molecules with four identical associating sites is obtained from

$$\chi_A(\mathbf{r}) = \frac{\sqrt{4n_0\zeta\Delta(\mathbf{r})+1}-1}{2} \tag{20}$$

with

$$\Delta(\mathbf{r}) = 4\pi K g^{hs}(\sigma, n_\alpha)\cdot(e^{\epsilon/k_B T}-1), \tag{21}$$

where K is a constant reflecting the volume available for bonding between two particles and $g^{hs}(\sigma, n_\alpha)$ is the contact value of hard-sphere pair correlation function at inhomogeneous conditions

$$g^{hs}(\sigma, n_\alpha) = \frac{1}{1-n_3} + \frac{n_2\sigma\zeta}{4(1-n_3)^2} + \frac{n_2^2\sigma^2\zeta}{72(1-n_3)^3}. \tag{22}$$

In the bulk limit, Eq. (22) reduces to the expression for the contact value of the radial distribution function for hard spheres.

With the intrinsic Helmholtz energy given by Eqs. (3), (6), and (19) for contributions from, respectively, ideal-gas, hard-sphere and associations, the Euler–Lagrange equation (2) now becomes

$$\mu - V_{\text{ext}}(\mathbf{r}) = k_B T \ln[\rho(\mathbf{r})\lambda^3]$$

$$+ k_B T \int d\mathbf{r}' \left(\sum_\alpha \frac{\partial \Phi}{\partial n_\alpha} \omega^{(\alpha)}(\mathbf{r} - \mathbf{r}') \right). \quad (23)$$

For spherical particles confined in microchannels, the density profiles are invariant in the z direction. The external potential due to the hard walls is equivalent to impose $\rho = 0$ outside of the boundaries.

The chemical potential in Eq. (23) can be calculated from that corresponding to a bulk fluid

$$\mu = k_B T \ln[\rho_b \lambda^3] + \Phi'(\rho_b), \quad (24)$$

where $\Phi'(\rho_b)$ is the derivative of the bulk residue Helmholtz energy density Φ with respect to the bulk density ρ_b. For hard spheres, $\Phi'(\rho_b)$ is calculated from the Carnahan–Starling equation of state and for associating spheres, it is calculated from SAFT. A comparison of Eqs. (23) and (24) yields the density profile in microchannels

$$\rho(x,y) = \rho_b \exp\left[\Phi(\rho_b) + \rho_b \Phi'(\rho_b) \right.$$

$$\left. - \int d\mathbf{r}' \left(\sum_\alpha \frac{\partial \Phi}{\partial n_\alpha} \omega^{(\alpha)}(\mathbf{r} - \mathbf{r}') \right) \right]. \quad (25)$$

As discussed in our previous works,[22,25] Eq. (25) can be solved numerically using the Picard-type iterative method. The weighted densities and the integrals in Eq. (25) are evaluated using Gauss formulas because they are improper integrals.

IV. RESULTS AND DISCUSSION

We have performed *NVT* simulations for neutral hard spheres of uniform size confined in a hard rectangular channel with fixed height $h = 9$ and length $l = 14$. The two-dimensional density profiles and the chemical potentials within the channel are calculated at the following averaged reduced densities: $\rho_{\text{av}}\sigma^3 = 0.42$, 0.53, 0.66, 0.72, 0.78, 0.87, and 0.93. Here the averaged density within the channel is defined as

$$\rho_{\text{av}} = \frac{N}{L \cdot H \cdot L_z}, \quad (26)$$

where N is the number of particles used in the simulation $L = (l+1)\sigma$, $H = (h+1)\sigma$, and L_z is the length of the simulation box in the z direction.

The reduced excess chemical potential of a hard sphere in the microchannel is related to the probability of successful insertions p by

$$\mu^{\text{ex}} = -k_B T \ln p. \quad (27)$$

In the original particle-insertion method proposed by Widom,[17] the test particle is identical to the real particles. In Table I, we present the probabilities of successful insertion using Widom's method at various average densities in the rectangular channel. Figure 1 presents the standard deviations in evaluation of these probabilities calculated from an error estimation method proposed by Flyvbjerg and Petersen.[27] Because the probability of successful insertion is

TABLE I. Monte Carlo simulation results for the probability of successful insertion using Widom's method, the excess chemical potentials (μ^* $\equiv \mu^{\text{ex}}_{\text{av}}/k_B T$) from Widom's method ($\mu^*_W$) and from the polynomial extrapolation using Eq. (1) (μ^*_P), the reduced R values in the polynomial fitting, and the reduced densities of the corresponding bulk fluid with the same chemical potential from μ^*_P.

$\rho_{\text{av}} \cdot \sigma^3$	p	μ^*_W	μ^*_P	R value	$\rho_b \sigma^3$
0.42	4.12×10^{-2}	3.19	3.19	1.0	0.445
0.53	8.93×10^{-3}	4.72	4.72	1.0	0.560
0.66	7.09×10^{-4}	7.25	7.25	1.0	0.693
0.72	1.51×10^{-4}	8.80	8.80	1.0	0.754
0.78	2.33×10^{-5}	10.67	10.68	1.0	0.814
0.87	7.00×10^{-7}	14.17	14.19	1.0	0.901
0.93	1.10×10^{-7}	16.02	15.97	0.9999	0.937

extremely low at high density, the numerical efficiency of Widom's method declines as the density increases. In this work, we measure the probability of insertion for a series of hard spheres with diameter d ranging from 0.55σ to σ. The excess chemical potential of the real sphere (with diameter σ) is extrapolated by best fitting of $\mu^{\text{ex}}(d)$ using Eq. (1). Figure 2 shows the reduced excess chemical potential as a function of the diameter of the testing particle at various average densities.

From the excess chemical potential calculated from the particle insertion method, we are able to determine the chemical potential and the density of the corresponding bulk fluid from

$$\mu^{\text{ex}}_{\text{av}} + k_B T \ln \rho_{\text{av}} = \mu^{\text{ex}}_b + k_B T \ln \rho_b \quad (28)$$

and an expression for the excess chemical potential of the bulk fluid μ^{ex}_b from the Carnahan–Starling equation of state[28]
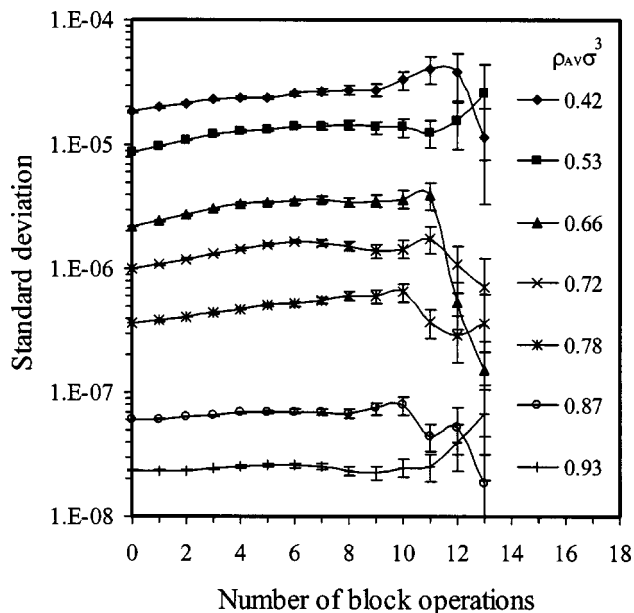

FIG. 1. The standard deviations in sampling the probability of successful particle insertion using Widom's method. The mean values of the insertion probabilities are listed in Table I.
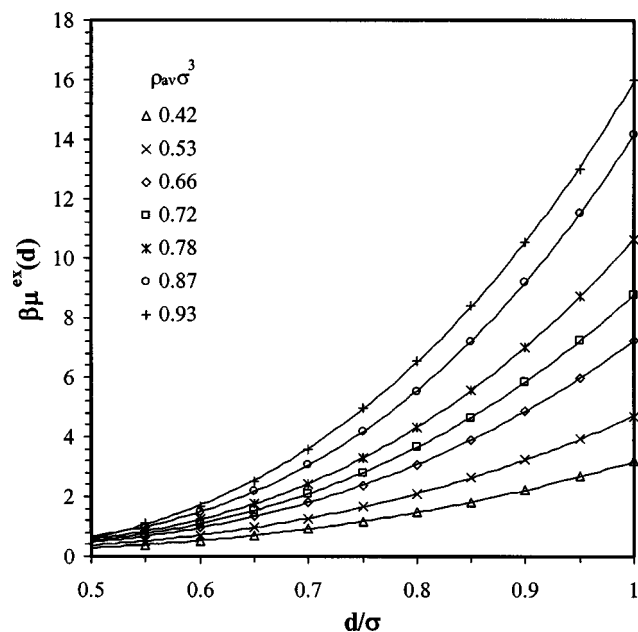
FIG. 2. The excess chemical potentials of testing particles of various diameters in a hard-sphere fluid confined in a rectangular channel with $l=14$ and $h=9$. The testing sphere is identical to the real hard sphere when $d/\sigma=1$.

$$\mu_b^{ex}/k_BT=\frac{\eta(8-9\eta+3\eta^2)}{(1-\eta)^3}. \tag{29}$$

In Eq. (29), $\eta=(\pi/6)\rho_b\sigma^3$ is the packing fraction of hard spheres. Table I presents the extrapolated excess chemical potentials at $d=\sigma$, the corresponding bulk densities, and the R-squared values of the polynomial fit using Eq. (1).

Figures 3(a) and 3(b) show the normalized density profiles $\rho(x,y)/\rho_b$ within the microchannel at two different averaged densities, $\rho_{av}\sigma^3=0.42$ and 0.93, respectively, corresponding to the lowest and highest densities investigated in this work. At the low density, the distribution of hard spheres within the microchannel is relatively uniform. The densities near the walls and corners are comparable to the contact values of the radial distribution function for uniform hard spheres at the same packing density. However, at the high density, the local densities at the corners are about two orders of magnitude larger than those in the middle, indicating that the particles are highly localized near the walls and corners. Figures 4(a) and 4(b) show the density profiles at the midplane along x and y directions ($x/\sigma=7$ and $y/\sigma=4.5$). Here the average densities are identical to those shown in Fig. 3. While the distribution of hard spheres at the midplane is invariant in x or y directions for the low-density case, remarkable difference is observed for the high-density case, indicating the effect of confinement is enhanced as density increases.

Figures 5(a) and 5(b) compare the normalized local number density profiles near the wall ($y/\sigma=0.0625$) and at the midplane ($y/\sigma=4.4875$) calculated from the Monte Carlo simulation to those predicted from the density functional theory. While the agreement between theory and simulation is excellent at low average density, the accuracy of the theory deteriorates as density increases and it becomes only
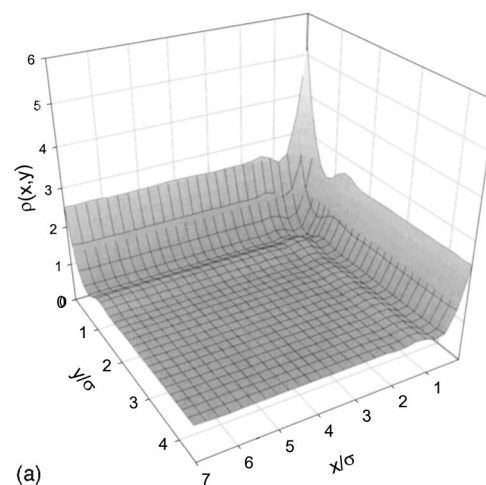
(a)
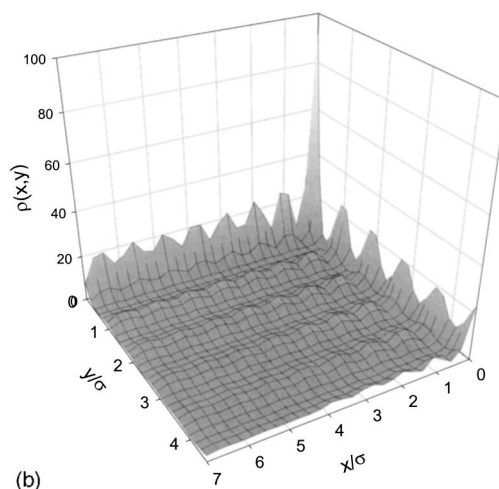
(b)

FIG. 3. The normalized density profiles $\rho(x,y)/\rho_b$ of a confined hard-sphere fluid in the rectangular channel as in Fig. 2 from NVT simulation. (a) $\rho_{av}\sigma^3=0.42$, (b) $\rho_{av}\sigma^3=0.93$. Because of the symmetry of the rectangular channel, the density profile in a quarter of the microchannel is presented.

semiquantitative near the freezing of hard spheres. The poor performance of the DFT at high density is probably due to the inaccuracy of the fundamental measure theory for highly confined systems. The failure of the fundamental measure theory at high density is because its Helmholtz energy functional diverges in the 0-dimensional limit. A possible improvement of the density functional theory is by imposing the exact free energy in the zero-dimension limit as proposed by Tarazona.[29]

We have applied the DFT theory to calculate density profiles in microchannels of other geometry and compared with simulation results from the literature. The structure of hard-sphere fluid confined in a corrugated channel was investigated using GCMC simulation by Schoen and Dietrich.[13] In Fig. 6 we sketch the corrugated hard channel system investigated in this work. The corrugated channel is composed of periodic arrays of parallel hard wedges. The corrugated substrate is characterized by the dihedral angle γ of the grooves, the lateral periodicity length S_x in the x direction and distance S_y between two opposite substrates. Figure 7 compares a slice of the density distribution evaluated
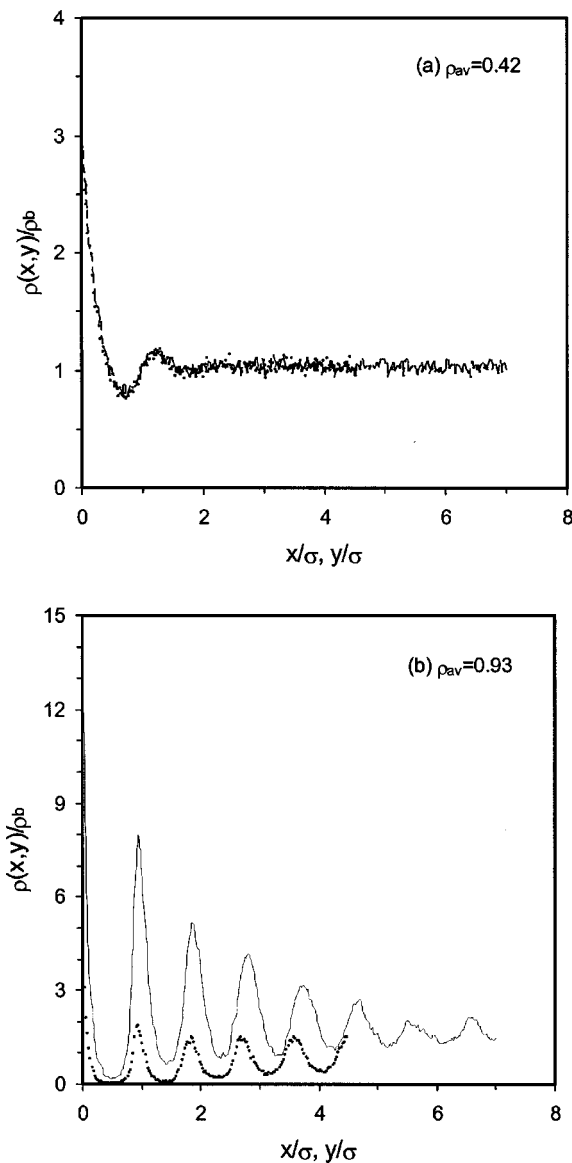
FIG. 4. The density profiles at the midplane of the rectangular channel from Monte Carlo simulation. Here the lines correspond to the density profiles at $h = 4.5$ and the points to those at $l = 7$. The rectangular channel is the same as that shown in Fig. 2.
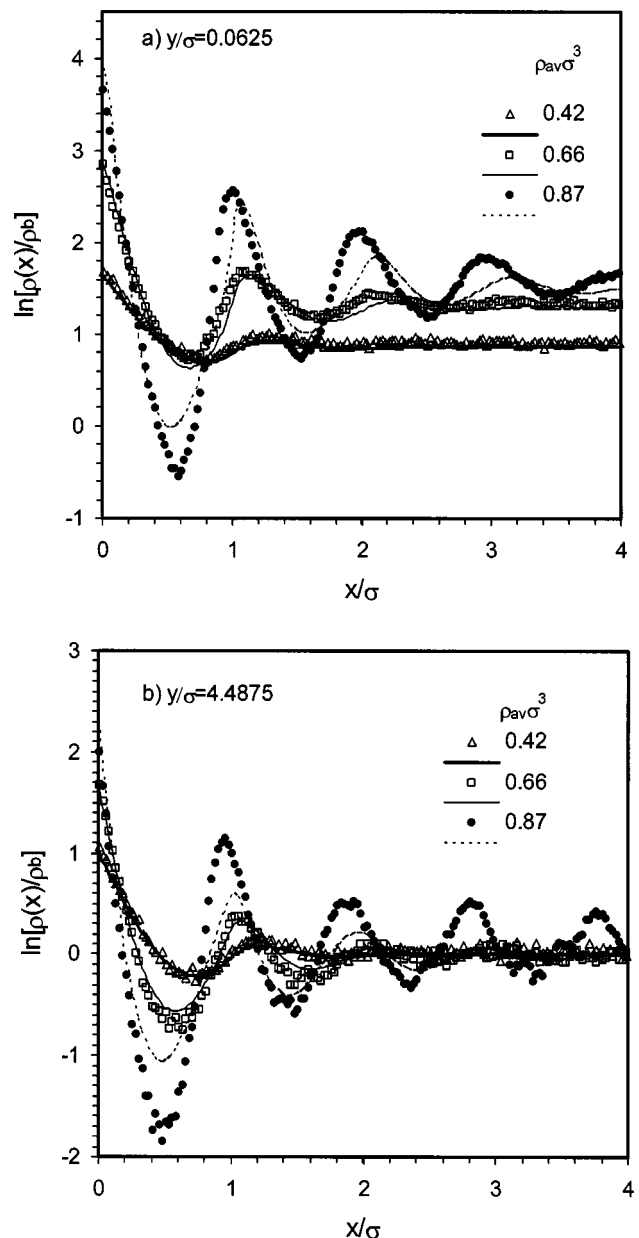

FIG. 5. (a) Density distributions of hard spheres near the wall of the rectangular channel calculated from Monte Carlo simulation (points) and from DFT (lines). (b) Same as (a) but at the midplane.

from the DFT and from the simulation[13] at $x/\sigma = 0.36$ and a reduced bulk density of 0.7016 in the hard corrugated channel for $\gamma = \pi/2$. In this case, the agreement between the theoretical prediction and molecular simulation is excellent. Figure 8 shows an overall local density profile in the $x-y$ plane calculated from the improved FMT. Similar to the distribution of hard spheres in rectangular channels, the density profile exhibits peaks along the corners and on each side of the corrugated walls.

The DFT was also used to investigate the effect of interparticle association on density distributions. Figure 9 shows the density profile of a four-sited associating hard-sphere fluid at temperature $1/T^* = 8$ and bulk density $\rho_b\sigma^3 = 0.7016$ in a rectangular channel. Here the reduced temperature is defined as $T^* = k_B T/\epsilon$, where ϵ is the site bonding energy. In this calculation, the volume parameter K in the SAFT theory is set to be $1.4849 \times 10^{-4}\sigma^3$. As for the hard-

sphere case, the rectangular channel has the dimension of $h = 9$ and $l = 14$. In contrast to the density profiles of confined neutral hard spheres as shown in Fig. 3, the local number densities at the corners are much smaller than those near the walls. The density distribution of associating hard spheres in the channel is determined by two competing effects: association and excluded volume. Because confinement restricts the associations, the particles are depleted from the walls or corners. On the other hand, the excluded volumes of the hard spheres leads to the accumulation of particles near a hard wall. While the former takes place only in associating fluids, the latter appears in both neutral and associating hard spheres. Finally, Fig. 10 shows the density profiles of four-sited associating hard spheres near the confining walls. As expected, the packing effect dominates the density distribu-
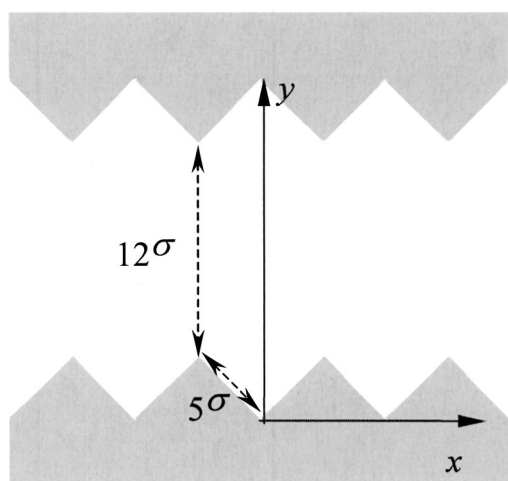
FIG. 6. Structure of the hard corrugated channel consisting of two opposite hard wedges of side length $S' = 10\sigma$, $S_y = 12\sigma$ and dihedral angle $\gamma = \pi/2$ in the (x,y) plane.

FIG. 8. The three-dimensional density profile for a hard-sphere fluid confined by the hard corrugated channel as shown in Fig. 5.

tion at low bonding energy (equivalently low $1/T^*$) and the association effect is important at high binding energy.

V. CONCLUSIONS

We have applied NVT ensemble Monte Carlo simulation and a newly proposed density functional theory to investigating the structures of confined spherical particles in rectangular and corrugated microchannels. We find that the density distribution of particles within microchannels is strongly affected by interparticle association and the geometry of confinement, especially at high densities. The prediction of density profiles from the density functional theory agrees well with simulation results for neutral hard spheres except near the freezing point.
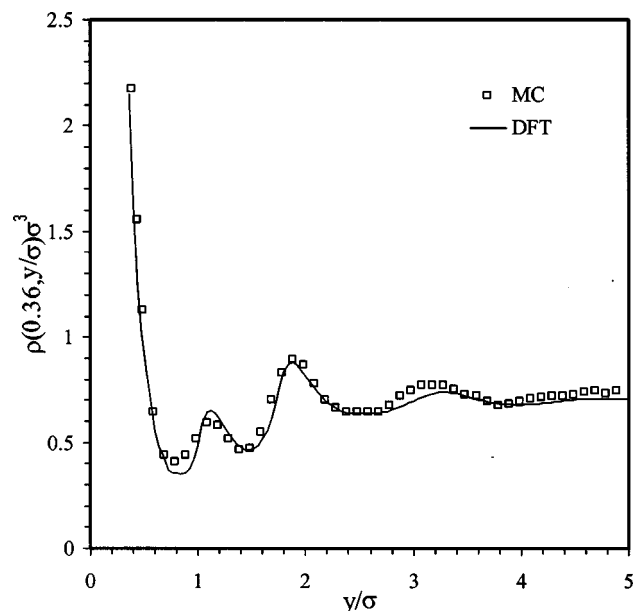
The chemical potential of hard spheres in a confined geometry can be effectively calculated using an extension of Widom's particle insertion method where the insertion probability is extrapolated from those for smaller particles. It might be interesting to use the NVT ensemble for studying the structural ordering of spherical particles in a confined geometry. While most previous applications of DFT for inhomogeneous fluids have been limited to systems of one-dimensional symmetry, this work demonstrates the feasibility of the application to multidimensional systems. Although similar applications had been reported for neutral hard

FIG. 7. Density distribution of hard spheres in the hard corrugated channel at $x/\sigma = 0.36$ and bulk density $\rho_b\sigma^3 = 0.7016$. Here the simulation results are from Schoen and Dietrich (Ref. 10).
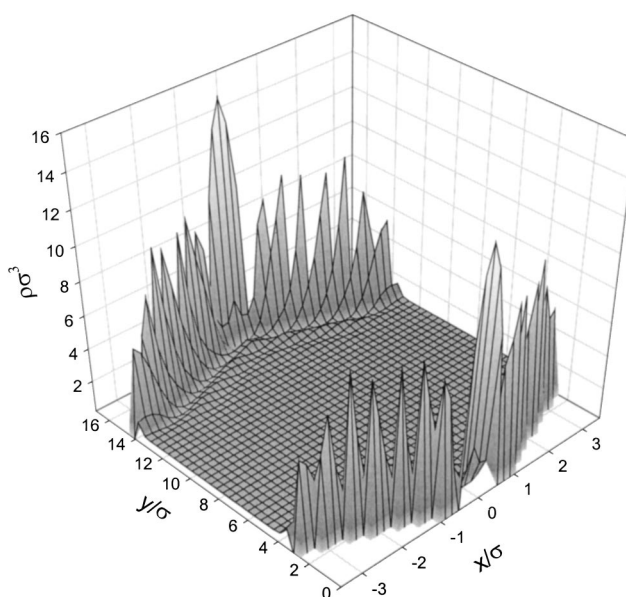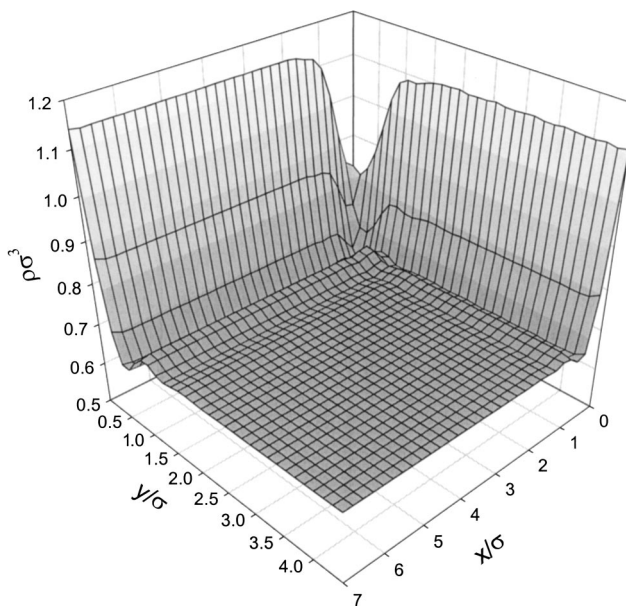

FIG. 9. Density distribution of a four-sited associating hard-sphere fluid in a rectangular channel with $l = 14$ and $h = 9$ at bulk density $\rho_b\sigma^3 = 0.7016$ and reduced temperature $1/T^* = 8$.
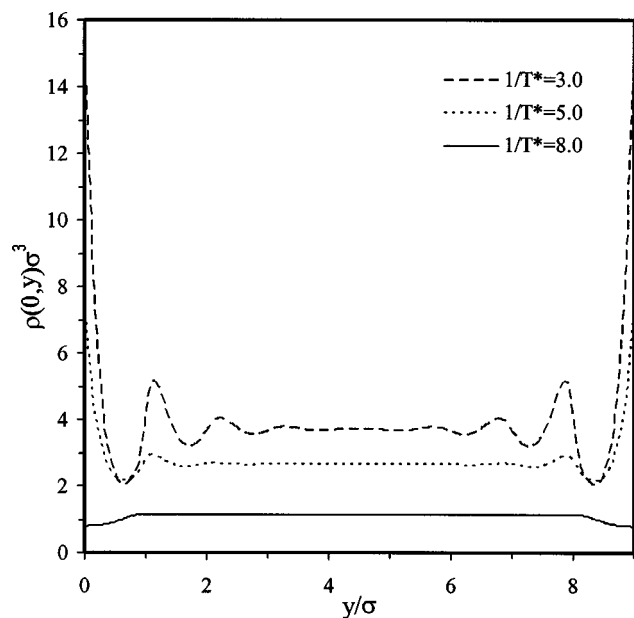
FIG. 10. The contact density distribution of four-sited associating hard spheres in a rectangular channel with $l=14$ and $h=9$ at three reduced temperatures and bulk density $\rho_b\sigma^3=0.7016$.

spheres, to our knowledge, no work has been published for the density profiles of two-dimensional associating fluids. In the future work, we plan to apply similar simulation and density functional theory to investigating wetting transitions and capillary condensations at heterogeneous surfaces.

The systems considered here represent simple models of colloidal dispersions confined in microchannels that are of interest to material chemists for the fabrications of colloid-based optical devices.[30,31]

ACKNOWLEDGMENTS

[1] S. M. Yang, H. Miguez, and G. A. Ozin, Adv. Funct. Mater. **12**, 425 (2002).
[2] M. S. Chun, Macromol. Theory Simul. **8**, 418 (1999).
[3] H. Lowen, J. Phys.: Condens. Matter **13**, R415 (2001).
[4] C. Bechinger and E. Frey, J. Phys.: Condens. Matter **13**, R321 (2001).
[5] H. K. Christenson, J. Phys.: Condens. Matter **13**, R95 (2001).
[6] B. K. Peterson, K. E. Gubbins, G. S. Heffelfinger, U. Marini, B. Marconi, and F. van Swol, J. Chem. Phys. **88**, 6487 (1988).
[7] A. Gonzalez, J. A. White, F. L. Roman, S. Velasco, and R. Evans, Phys. Rev. Lett. **79**, 2466 (1997).
[8] F. Porcheron, M. Schoen, and A. H. Fuchs, J. Chem. Phys. **116**, 5816 (2002).
[9] M. Calleja, A. N. North, J. G. Powles, and G. Rickayzen, Mol. Phys. **73**, 973 (1991).
[10] G. B. Woods and J. S. Rowlinson, J. Chem. Soc., Faraday Trans. 2 **85**, 765 (1989).
[11] D. Henderson, S. Sokolowski, and D. Wasan, Phys. Rev. E **57**, 5539 (1998).
[12] K. Jagannathan and A. Yethiraj, J. Chem. Phys. **116**, 5795 (2002).
[13] M. Schoen and S. Dietrich, Phys. Rev. E **56**, 499 (1997).
[14] W. A. Curtin and N. W. Ashcroft, Phys. Rev. A **32**, 2909 (1985).
[15] W. R. Smith and H. L. Vortler, Chem. Phys. Lett. **249**, 470 (1996).
[16] R. Radhakrishnan and K. E. Gubbins, Mol. Phys. **96**, 1249 (1999).
[17] B. Widom, J. Chem. Phys. **39**, 2802 (1963).
[18] Y. Rosenfeld, Phys. Rev. Lett. **63**, 980 (1989).
[19] Y. Rosenfeld, Phys. Rev. A **42**, 5978 (1990).
[20] T. Boublik, J. Chem. Phys. **53**, 471 (1970).
[21] G. A. Mansoori, N. F. Carnahan, K. E. Starling, and T. W. Leland, Jr., J. Chem. Phys. **54**, 1523 (1971).
[22] Y. X. Yu and J. Z. Wu, J. Chem. Phys. **117**, 10156 (2002).
[23] S. Labik and W. R. Smith, Mol. Phys. **88**, 1411 (1996).
[24] H. Reiss, H. L. Frisch, and J. L. Lebowitz, J. Chem. Phys. **31**, 369 (1959).
[25] Y. X. Yu and J. Z. Wu, J. Chem. Phys. **116**, 7094 (2002).
[26] W. G. Chapman, K. E. Gubbins, G. Jackson, and M. Radosz, Fluid Phase Equilib. **52**, 31 (1989).
[27] H. Flyvbjerg and H. G. Petersen, J. Chem. Phys. **91**, 461 (1989).
[28] N. F. Carnahan and K. E. Starling, J. Chem. Phys. **51**, 635 (1969).
[29] P. Tarazona, Phys. Rev. Lett. **84**, 694 (2000).
[30] G. A. Ozin and Y. San Ming, Adv. Funct. Mater. **11**, 95 (2001).
[31] Y. D. Yin, Y. Lu, B. Gates, and Y. N. Xia, J. Am. Chem. Soc. **123**, 8718 (2001).